Crosshole Electromagnetic Responses of Multiple Thin Conductors

EM 1.5

Qiang Zhou, Norman E. Goldstein, Lawrence Berkeley Lab; and Alex Becker, University of California, Berkeley

Summary

The crosshole audiofrequency electromagnetic response of vein-type conductors has been studied numerically using an integral equation method. A modeling program has been developed and tested to calculate the fields due to multiple thin conductors embedded in a conductive host rock. Both electric and magnetic dipole downhole sources can be treated. The purpose of the study is to investigate the detectability and characterization of thin conductors such as mineralized veins and fracture zones missed in drilling.

A number of tests cases have been run to check the accuracy of the code, and to study the effects of the interactions between conductors. We find that coupling effects between conductors may enhance or reduce the secondary field compared to the simple additive fields of the individual conductors. The interactions depend on the geometry of conductors in relation to the source/detector. The program is very efficient, but is presently limited to non-intersecting, homogeneous conductors.

Introduction

Current interest in mineral exploration and fracture mapping has prompted many studies on the use of surface-to-borehole and crosshole electromagnetic techniques to search for tabular conductors. Of particular interest to us is the problem of detecting and characterizing vein-type conductors missed in drilling. In the case where a single hole is available, in-hole VHF pulse radar and ultrasonic acoustic techniques have been considered as ways of searching for reflectors (*Chang* et al., 1984). The detection of tabular 3D conductors using surface-to-borehole controlled-source AMT has been studied by means of numerical models (*West* and *Ward*, 1988). In the case of two or more boreholes, both ultrasonic acoustic wave tomography (*King* et al., 1984; *Peterson* et al., 1985) and radar frequency electromagnetic tomography (*Ramirez* et al., 1982) have been used to image tabular conductive features located between strings of transmitters and detectors in separated holes.

Our study has concentrated on the use of subsurface audiofrequency electromagnetics (frequency range of 300 Hz to 10 kHz) for the detection of conductive veins embedded in a less conductive host rock. Previously developed 3-D numerical modeling programs (*Lee* et al., 1981; *Xiong* et al., 1986, among others) have limitations: they require an enormous amount of computing time, are limited to only surface sources/detectors, and/or can handle a single conductive target (*Zhou* et al., 1987).

Figure 1 gives a schematic description of the problem under study. From a geological perspective it includes fault-offset veins, or, as shown here, fault-offset massive sulfide lenses. Both fissure-filling veins and massive sulfide lenses can be treated as segments of thin rectangular bodies for this study. Each body is defined by a set of geometrical parameters (Fig. 2) and a fixed thickness-conductivity product (the sheet conductance), which in most geological situations ranges from a fraction of a Siemen to over 100 Siemens. The algorithm can be extended to an inhomogeneous conductor, but this has not yet been programmed.

The mathematical formulation and numerical solution

(1) The thin conductor model

The mineral veins are represented by rectangular thin-sheet conductors (two in the case shown in Fig. 2) of size a_i by b_i, i=1,2...ns, where ns is the number of targets. The tops and bottoms of the rectangular conductors are horizontal, and they are assumed to be thin relative to the EM wavelength so that only the conductances, τ_i, are important. This simplification is justified if the tangential electrical field $\mathbf{E}_s$ on the thin conductor varies slightly across its full thickness.

The conductors are located in a half space of conductivity σ_2. Above the half-space is an overburden with conductivity σ_1 and thickness D. The strike angle of the i-th sheet is denoted by γ_i and its dip angle by β_i. The coordinates of the center of the top edge are (X_{1i}, X_{2i}, H_i), where H_i is the depth to the horizontal top of the i-th fracture from the surface. The source, at a depth of H_{tx}, is harmonic in time ($e^{i\omega t}$). The depth of the receiver is represented by H_{rx}. In the crosshole cases, the separation between transmitting and receiving holes is X_{ch}, (i.e., both holes are vertical), and transmitter and detector are at the same elevation for each measurement. In the single-hole case, not treated here, the source and the receiver are separated by a fixed vertical distance L for each point of measurement.

In these calculations we use a vertical magnetic dipole transmitter with moment of one. Displacement currents are neglected, and the magnetic permeability, μ_0, is assumed to have the free space value. In addition, the boreholes are assumed to have zero diameter and have no influence on the fields.

(2) The derivation of the integral equations and their solution

The approach used to calculate the frequency-domain magnetic field responses is follows from the algorithm developed by Weidelt (1981) who calculated the magnetic field anomaly due to a thin conductor for source and receiver in the air. We have reformulated the algorithm to investigate the EM responses from multiple thin conductors and subsurface sources and receivers.

Beginning with Maxwell's equations and the assumption that the displacement current is negligible, one arrives at the following integral equation for the tangential electric fields on the i-th thin conductor

$$\mathbf{E}_{s_i}(\mathbf{r}_0) = \mathbf{E}_{ns_i}(\mathbf{r}_0) - i\omega\mu_0 \sum_{j=1}^{ns} \int_{s_j} \tau_j(\mathbf{r})\, g_{sji}(\mathbf{r}_0/\mathbf{r}) \cdot \mathbf{E}_{s_j}(\mathbf{r}) ds, \qquad (1)$$

where g_{sji} is the Green's dyadic function relating the electric field on the i-th sheet to that on the j-th sheet. Similarly, the magnetic field at any point in the space is given by

$$\mathbf{H}(\mathbf{r}_0) = \mathbf{H}_n(\mathbf{r}_0) + \sum_{j=1}^{ns} \int_{s_j} \tau_j(\mathbf{r})\, \mathbf{E}_{s_j}(\mathbf{r}) \cdot \nabla_0 \times g(\mathbf{r}/\mathbf{r}_0) ds. \qquad (2)$$

Here $\mathbf{E}_s$ is the tangential electric field on the sheet, and $\mathbf{E}_{ns}$ is the

incident tangential electric field on it. Likewise, **H** is the total magnetic field and $\mathbf{H}_n$ is the incident (primary) magnetic field at the point of observation. $g(r_0/r)$ is the Green's dyadic functions relating the tangential current distribution on the sheet with the electric fields everywhere. The conductance $\tau(r)$ is the sheet conductivity-thickness product, which will be assumed to be a constant on each thin sheet.

Both the incident fields $\mathbf{E}_n$ and $\mathbf{H}_n$ and the Green's dyadic functions g and $g_{s,i}$ are related to the dipole fields in a layered medium (3 layers considered here) and are easy to evaluate (*Lajoie* et al., 1976; *Johannsen* et al., 1979; and *Weidelt*, 1981). After the targets are discretized and $\mathbf{E}_n$ and g_s are calculated, equation (1) is then solved for $\mathbf{E}_s$, which is then used in equation (2) together with the calculated $\mathbf{H}_n$ and $\nabla_0 \times g$ to obtain **H** at the receiver sites. For the examples shown here, we display only the in-phase and quadrature components of the vertical secondary magnetic field; i.e., the vertical component of the integral term in equation (2).

(3) Accuracy

Several numerical tests were made to check code accuracy. The first test was to check the convergence of the in-phase and quadrature fields as the number of surface elements (s_j) that make up conductor increases. The second test was to check reciprocity by interchanging source and detector. Thirdly, we checked the code by running several cases for two identical, parallel conductors at decreasing separations. In the limit; i.e., nearly zero separation, their EM responses are the same as from a single conductor with twice the conductance. Lastly, using a single conductor we compared the results to those generated using existing programs (*Dyck* et al., 1980; *Zhou* et al., 1987) for both electric and magnetic dipole sources.

On the basis of these tests we have concluded that the code is self-consistent and compatible with others.

Examples of the interactions between conductors

Two models are shown that illustrate the enhancement and reduction of the secondary responses due to the presence of multiple conductors. The calculations are shown for 3 kHz because the secondary fields are relatively large at this frequency. Figures 3a and 3b show the secondary magnetic fields when two identical vertical thin sheets lie between source and receiver holes. As we can see, the response from both conductors is much less than the sum from two individual conductors. Here, the interaction between the two targets weakens the total secondary response. On the other hand, placing the source and receiver holes midway between two vertical conductors (Fig. 4a), the secondary field for the two conductors is much larger than the sum of the responses of two single conductors. This can be explained as due to additional secondary currents on the two conductors because of a mutual inductive coupling effect. These two examples reveal that the total secondary field generally cannot be approximated by simple addition of the individual responses. Whether multiple targets increase or decrease the total secondary field depends on the relative positions of the source, receiver, and the conductors. Comparing Figures 3 and 4, we can also see that the quadrant of the secondary field depends on where the conductors are in relation to the holes. The quadrant and amplitudes of the responses are also frequency dependent.

Conclusions

The test runs confirm the accuracy and efficiency of the code, and illustrate that electromagnetic effects between conductors may either enhance or reduce the amplitude responses compared to the simple additive responses of the individual conductors. The numerical examples also show that the quadrant of the secondary magnetic field depends on the location of the conductor(s) relative to the source-detector holes.

EM waves at audiofrequencies have a large depth of penetration, and it should be possible to develop suitable borehole instruments. The advantage of a vertical detector, as simulated in these calculations, is that the vertical component of the natural audiofrequency electromagnetic field (natural noise) is very small; much smaller than the man-made signal and theoretically zero where the earth is horizontally layered or homogeneous (*West* and *Ward*, 1988). In the case where transmitter and detector are at the same elevation in their respective boreholes, the primary vertical magnetic field is as large or larger than the secondary (anomalous) field due to the conductors, and it varies with depth below the overburden layer. For these reasons, and the need for broad-band measurements, a time-domain system seems like a more logical approach to crosshole EM.

The computing time for 20 crosshole source-receiver positions in a model containing two thin conductors of finite dimensions, buried beneath an overburden layer is about 60 seconds on an IBM 3090 computer.

Acknowledgments

We wish to thank H. F. Morrison and K. H. Lee for their assistance in the numerical modeling. This work is supported by the Assistant Secretary for Conservation and Renewable Energy, Office of Renewable Technology, Division of Geothermal and Hydropower Technologies of the U.S. Department of Energy under Contract No. DE-AC03-76SF00098.

References

Dyck, A. B., Bloore, M. and Vallee, M. A., 1980, User manual for programs PLATE and SPHERE: Res. in Applied Geophysics. No. 14, Univ. of Toronto, Toronto.

Johannsen, H. K. and Sorensen, K., 1979, Fast Hankel transforms: Geophysical Prospecting, **27**, 876-901.

King, M. S., Myer, L. R. and Rezowalli, J. J., 1984, Cross-hole acoustic surveying in basalt: Lawrence Berkeley Laboratory, LBL-17314.

Lajoie, J. J. and West, G. F., 1976, Electromagnetic response of a conductive inhomogeneity in a layered earth: Geophysics, **41**, 1133-1156.

Lee, K. H., Pridmore, D. F. and Morrison, H. F., 1981, A hybrid three-dimensional electromagnetic modeling scheme: Geophysics, **46**, 796-805.

Peterson, J. E., Paulsson, B. N. P. and McEvilly, T. V., 1985, Applications of algebraic reconstruction techniques to crosshole seismic data: Geophysics, **50**, 1566-1580.

Ramirez, A. L., Deadrick, F. J. and Lytle, R. J., 1982, Cross-borehole fracture mapping using electromagnetic geo-tomography: Lawrence Livermore National Laboratory, UCRL-53255.

Weidelt, P., 1981, Report on dipole induction by a thin plate in a conductive half-space with and overburden: Federal Institute for Earth Science and Raw Materials, Hannover, Germany.

West, R. C. and Ward, S. H., 1988, The borehole controlled-source audiomagnetotelluric response of a three-dimensional fracture zone: Geophysics, **53**, 215-230.

Xiong, Z., Luo, Y., Wang, S. and Wu, G., 1986, Induced-polarization and electromagnetic modeling of a three-dimensional body buried in a two-layered anisotropic earth: Geophysics, **51**, 2235-2246.

Zhou., Q., Becker, A., Goldstein, N. E., Morrison, H. F. and Lee, K. H., 1987, Fracture detection using subsurface electromagnetic techniques: Proceedings of the 28-th U.S. Rock Mechanics Symposium, A. A. Balkema, Rotterdam, 5-17.

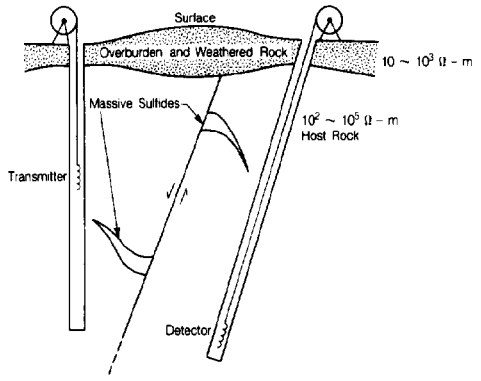

FIG. 1. Crosshole EM borehole survey to detect conductors missed in drilling.

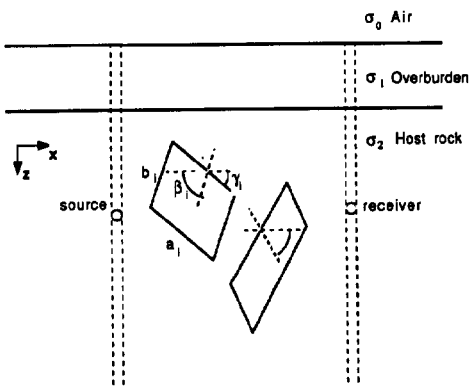

FIG. 2. Parameters used in multiple sheet code.

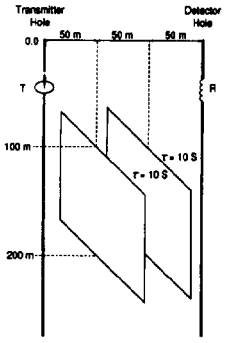

FIG. 3a. Two identical conductors between boreholes.

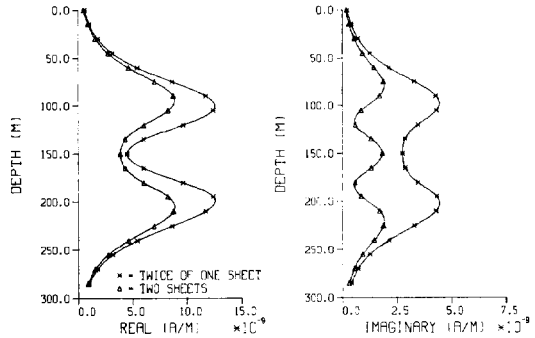

FIG. 3b. In-phase and quadrature responses of case in Figure 3a at 3 kHz.

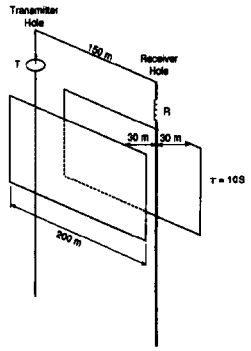

FIG. 4a. Two identical conductors outside plane of two boreholes.

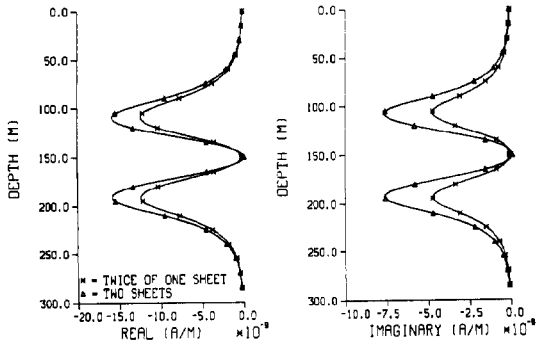

FIG. 4b. In-phase and quadrature responses of case in Figure 3a at 3 kHz.